Escherichia coli Methionine Aminopeptidase: Implications of Crystallographic Analyses of the Native, Mutant, and Inhibited Enzymes for the Mechanism of Catalysis[†,‡]

W. Todd Lowther,[§] Allen M. Orville,[§] David T. Madden,[§] Sejin Lim,[||] Daniel H. Rich,[||] and Brian W. Matthews*[,§]

Institute of Molecular Biology, Howard Hughes Medical Institute and Department of Physics, 1229 University of Oregon, Eugene, Oregon 97403, and Department of Chemistry and School of Pharmacy, University of Wisconsin—Madison, 425 North Charter Street, Madison Wisconsin 53706

Received March 24, 1999

ABSTRACT: By improving the expression and purification of *Escherichia coli* methionine aminopeptidase (eMetAP) and using slightly different crystallization conditions, the resolution of the parent structure was extended from 2.4 to 1.9 Å resolution. This has permitted visualization of the coordination geometry and solvent structure of the active-site dinuclear metal center. One solvent molecule (likely a μ-hydroxide) bridges the trigonal bipyramidal (Co1) and octahedral (Co2) cobalt ions. A second solvent (possibly a hydroxide ion) is bound terminally to Co2. A monovalent cation binding site was also identified about 13 Å away from the metal center at an interface between the two subdomains of the protein. The first structure of a substrate-like inhibitor, (3*R*)-amino-(2*S*)-hydroxyheptanoyl-L-Ala-L-Leu-L-Val-L-Phe-OMe, bound to a methionine aminopeptidase, has also been determined. This inhibitor coordinates the metal center through four interactions as follows: (i) ligation of the N-terminal (3R)-nitrogen to Co2, (ii, iii) bridging coordination of the (2S)-hydroxyl group, and (iv) terminal ligation to Co1 by the keto oxygen of the pseudo-peptide linkage. Inhibitor binding occurs with the displacement of two solvent ligands and the expansion of the coordination sphere of Co1. In addition to the tetradentate, bis-chelate metal coordination, the substrate analogue forms hydrogen bonds with His79 and His178, two conserved residues within the active site of all MetAPs. To evaluate their importance in catalysis His79 and His178 were replaced with alanine. Both substitutions, but especially that of His79, reduce activity. The structure of the His79Ala apoenzyme and the comparison of its electronic absorption spectra with other variants suggest that the loss in activity is not due to a conformational change or a defective metal center. Two different reaction mechanisms are proposed and are compared to those of related enzymes. These results also suggest that inhibitors analogous to that reported here may be useful in preventing angiogenesis in cancer and in the treatment of microbial and fungal infections.

Methionine aminopeptidase (MetAP)[1] removes the ubiquitous N-terminal methionine from proteins. The enzyme preferentially hydrolyzes both protein and peptide substrates that have a small, uncharged amino acid in the penultimate position (*1*, *2*). This family of enzymes is divided into two classes (type I and type II), the latter characterized by an insertion of approximately 60 residues within the aminopeptidase domain (*3*). Despite this insertion and other differences, all MetAP crystal structures appear to have similar architecture (*4*−*6*). The active sites, which are also similar, are located at the interface between pseudo 2-fold related N- and C-terminal subdomains (*4*). The structure of the prototypical *Escherichia coli* enzyme (eMetAP) showed that conserved residues, contributed by both subdomains of the protein, coordinate a dinuclear metal center essential for activity (*1*, *4*, *7*). This structure, however, determined at 2.4 Å resolution, did not identify a metal-bridging solvent ligand as seen in other MetAPs and dinuclear metal centers with comparable metal−metal distances (2.9−3.5 Å) (*8*). Such a μ-hydroxo or μ-aquo ligand has been proposed to be the attacking nucleophile in other aminopeptidases (*9*−*11*) and metallohydrolases (*12*, *13*). Historically, Co(II) has been used to study the properties of this enzyme because of its ability to reconstitute apoenzyme with high activity and its unique spectral characteristics (*1*, *14*). A recent report, however, suggests that the in vivo activity of type I yeast MetAP (yMetAP-I) is mediated by Zn(II) (*15*).

[†] This work was supported in part by the National Research Service Award F32-GM17536 (W.T.L.) and Research Grant GM20066 (B.W.M.) from the National Institutes of Health.

[‡] The coordinates have been deposited in the Brookhaven Protein Data Bank under the accession numbers 2MAT, 3MAT, and 4MAT.

* To whom correspondence should be addressed. E-mail: brian@uoxray.uoregon.edu. Phone: (541) 346-2572. Fax: (541) 346-5870.

[§] University of Oregon.

[||] University of Wisconsin—Madison.

[1] Abbreviations: AQC, 6-aminoquinolyl-*N*-hydroxysuccinimidylcarbamate; AHHpA, (3*R*)-amino-(2*S*)-hydroxyheptanoic acid; creatinase, creatine amidinohydrolase; MetAP, methionine aminopeptidase; eMetAP, *E. coli* MetAP; hMetAP-II, human MetAP type II; yMetAP-II, yeast MetAP type II; pfMetAP, *P. furiosis* MetAP; Nle, norleucine; LeuAP, leucine aminopeptidase; ProAP, aminopeptidase P; Mes, 2-(*N*-morpholino)ethanesulfonic acid; Hepes, *N*-2-hydroxyethylpiperazine-*N*′-2-ethanesulfonic acid; DMSO, dimethyl sulfoxide; EDTA, ethylenediaminetetracetic acid.

10.1021/bi990684r CCC: $18.00
Published on Web 05/26/1999

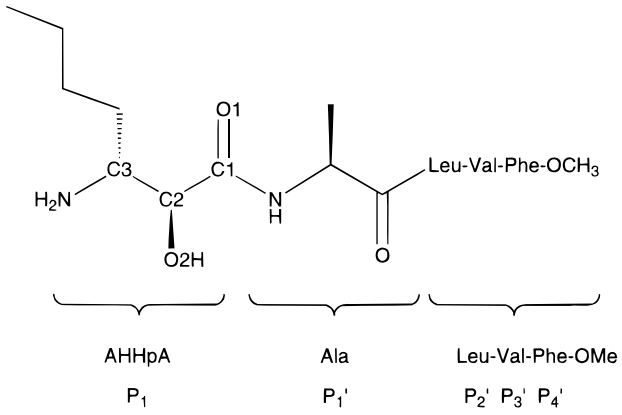

FIGURE 1: Structure and labeling scheme for the inhibitor of MetAP used in this report. Substitutions to the structure of bestatin, a natural product, were made to match the substrate specificity of MetAP. The norleucine analogue, AHHpA, at the P_1 position replaces the N-terminal methionine of a substrate rendering it nonhydrolyzable. The P_1' residue was changed to Ala [nomenclature of Schecter and Berger (*25*)].

Human MetAP-II has been shown to be the molecular target (*16*, *17*) of the potent anti-angiogenesis agents fumagillin, ovalicin, and a related compound, TNP-470, currently in cancer clinical trials (*18*). His79 in eMetAP and the equivalent residues in the human (hMetAP-II) and yeast (yMetAP-II) enzymes have been biochemically (*14*, *19*) and structurally (*6*) shown to be the site of covalent modification by this class of compounds. These observations imply that the processing of certain proteins or peptides by MetAP may be required for angiogenesis and the vascularization of tumors (*20*, *21*). These studies also suggest that His79 and another conserved histidine (His178 in eMetAP), both of which are close to the metal center, may play a role in catalysis.

In an effort to understand the mechanism of action of MetAP, we have followed a multifaceted approach, including the development and structural analysis of inhibitor complexes, the construction and analysis of mutants, improvement in the resolution of the parent structure, as well as comparisons with LeuAP (*9*, *10*, *22*, *23*), creatinase (*24*), and ProAP from *E. coli* [(*11*) also known as AMPP].

MATERIALS AND METHODS

Crystallization, Data Collection, and Refinement. The bestatin-based inhibitor (3*R*)-amino-(2*S*)-hydroxyheptanoyl-L-Ala-L-Leu-L-Val-L-Phe-OMe (Figure 1) was prepared by a stepwise solution strategy (*26*, *27*). The stereochemistry of the inhibitor was predominantly (3*R*,2*S*) although about 12% of the (3*R*,2*R*) enantiomer was present.

Recombinant eMetAP (Arg175Gln) was prepared in the same manner as previously reported and stored at −80 °C in aliquots containing 25 mM Hepes, pH 6.8, 25 mM K_2SO_4, 100 mM NaCl, 1 mM $CoCl_2$, and 15 mM methionine (*14*). The background Arg175Gln mutation was included to remove a secondary thrombin cleavage site within a surface loop. Crystals of the Co(II)-substituted enzyme were grown at room temperature by vapor diffusion in 20−30 μL sitting drops after mixing the protein, 12 mg/mL solution in storage buffer containing 48.8 mM *N*-octanoyl sucrose (Calbiochem-Novabiochem Corp., La Jolla, CA), 1:1 with well solutions containing 24−26% PEG 4000, 0.1 M Hepes, pH 7.0−7.2, and fresh 2 mM $CoCl_2$. Crystals of the inhibitor complex were obtained by incubating the enzyme as above at room temperature for 5 min with a 20-fold molar excess of the inhibitor dissolved in DMSO. The final inhibitor:enzyme ratio was 10:1 (1% DMSO) after mixing the preformed complex with well solution (0.1 M Mes, pH 6.1, 2 mM $CoCl_2$, and 27−31% PEG 4000). Crystals of the His79Ala mutant were obtained by mixing the apoenzyme retaining the C-terminal His-tag (*14*) (6.7 mg/mL, 20 mM DTT in storage buffer without cobalt) with an equal volume of well solution (22−27% PEG 3400, 0.1 M Hepes, pH 7.0, and 200 mM NaCl). Diffraction quality crystals were obtained after macroseeding into 20μL hanging drops.

X-ray diffraction data were collected by the oscillation method on either a Raxis II or IV with a Rigaku rotating anode source. The raw data were merged and scaled using DENZO and SCALEPACK (*28*). The holoenzyme and the inhibitor complex data were collected at room temperature. Data for the His79Ala mutant were collected at −170 °C after equilibrating the crystal in 25% glycerol, 0.2 M NaCl, and 0.1 M Hepes, pH 7.0 for 30 min. Because of variations of several angstroms in the cell dimensions (Table 1), it was necessary to use molecular replacement (*29*) to facilitate the determination of the higher-resolution holoenzyme structure as well as that of the mutant and the inhibitor complex. After placing the starting model without the cobalt atoms (*4*) into

Table 1: X-ray Data Collection and Refinement Statistics

	holo-enzyme[a]	holo-enzyme[b]	inhibitor complex	Apo-His79Ala
space group	$P2_1$	$P2_1$	$P2_1$	$P2_1$
cell parameters				
a (Å)	39.0	39.3	39.3	38.7
b (Å)	61.7	67.7	65.2	68.3
c (Å)	54.5	48.9	51.4	55.5
β (deg)	107.3	111.2	106.1	106.0
data statistics[c]				
resolution range (Å)	52.0−2.4	35.5−1.9	37.8−2.1	28.8−2.0
collected reflections		94 123	45 928	48 052
unique reflections	8387	18 444	13 762	16 062
completeness (%)	82	100 (100)	94.0 (92.9)	85.2 (70.8)
$<I/\sigma(I)>$		22.7 (6.1)	20.5 (4.8)	22.4 (4.4)
R_{sym} (%)		7.7 (25.1)	7.6 (25.5)	4.7 (21.0)
refinement statistics[d]				
R (%)	18.2	15.5	15.6	18.4
Δ_{bonds} (Å)		0.012	0.013	0.012
Δ_{angles} (deg)		2.3	2.3	2.4
$\Delta_{trig\ planes}$ (Å)		0.008	0.008	0.008
Δ_{planes} (Å)		0.013	0.013	0.012
average thermal factors				
protein atoms (Å^2)		22.4	23.2	23.0
solvent (Å^2)		31.5	32.6	34.1
inhibitor atoms (Å^2)			36.3	
Co1, Co2 (Å^2)		15.4	17.1	
Co3 (Å^2)		56.9		
Na^+ (Å^2)		13.0	28.9	16.7

[a] These data are for the original determination of the holoenzyme structure (*4*) and are included for reference and to show the differences in cell dimensions and in resolution compared to the present studies. [b] This report. [c] $<I/\sigma(I)>$ is the root-mean-square value of the intensity measurements divided by their estimated standard deviation. R_{sym} gives the average agreement between independently measured intensities. The values for the highest resolution shells are given in parentheses: holoenzyme (1.90−1.97 Å), complex (2.10−2.17 Å), His79Ala (2.00−2.07 Å). [d] *R* is the crystallographic residual following refinement. Δ_{bonds}, Δ_{angles}, $\Delta_{trig\ planes}$, and Δ_{planes} give the average departure from ideal values of the bond lengths, bond angles, trigonal planes, and other planar groups of atoms.

the new unit cell of the holoenzyme, it was refined by (i) rigid-body refinement using first the entire model and then 20 smaller secondary structural elements, (ii) the assignment of different rotamers to several amino acid side chains, (iii) the inclusion of amino acid side chains not seen previously, and (iv) the addition of water molecules to 3σ positive difference features in an $F_o - F_c$ electron density map. After each session of building in CHAIN (*30*) or O (*31*), the model was refined with TNT (*32*). The 1.9 Å resolution model of the holoenzyme was used as the molecular replacement search model for the determination of the inhibitor complex and the His79Ala mutant. The refinement parameters for the inhibitor were based on the small-molecule crystal structure of bestatin (*33*). The His79Ala model required additional modifications at the C-terminus due to extensive interactions with the active site of a symmetry-related molecule. In the final stages, all models were refined with unit occupancy and correlated thermal factor restraints (*34*).

Mutagenesis and Activity Analysis. The His79Ala mutant was generated as previously reported (*14*). The His178Ala mutant, in the Arg175Gln "wild-type" background, was created and purified in an analogous manner using the same 5′-and 3′-end primers and the following mutagenic primers: 5′-CGG TTC TTC AGC GAA GCC CTG GCC G-3′ and 5′-TGA AGA ACC GCA GGT GCT GCA C-3′. The holoenzyme and the His79Ala and His178Ala mutant enzymes used for activity assays were stored in their metal-free form following treatment with 5 mM EDTA and passage through a gel filtration column equilibrated with 50 mM Hepes, pH 7.5, and 100 mM KCl, which also removed the methionine present in previous steps in the purification scheme. Enzyme used to ascertain the activity levels in the presence of Zn(II) was incubated overnight (>16 h) on ice in the presence of 12 mM EDTA (24 mg/mL protein) prior to analysis.

All enzymes were freshly diluted with ice-cold 20 mM Hepes, pH 7.1, prior to a 5 min preincubation with buffer containing freshly prepared $CoCl_2$ or $ZnCl_2$ at 30 °C. After the addition of substrate, the final reaction conditions were 50 mM Hepes, pH 7.1; 50 mM KCl; 0.1−0.2 mM $CoCl_2$ or 0.1−1 mM $ZnCl_2$; 4 mM substrate; and 0.05−5 mg/mL enzyme. Experiments directly comparing activity in the presence of Co(II) or Zn(II) also contained 24 μM EDTA. The reaction was quenched after 10 min by a 10−100-fold dilution with 10 mM EDTA, pH 8.8. The release of the N-terminal norleucine from the substrate, Nle-Ala-Ala-Glu-Glu, was determined by derivatization with AQC (*35*) in the ratio 1:3:1 (sample:Waters borate buffer:AQC, AccQ-Fluor Reagent Kit, Waters). A 50 μL aliquot of the sample was loaded onto a Beckman Gold HPLC/autosampler system fitted with a 5 μm, 4.6 mm × 15 cm Beckman ODS Ultrasphere column. The derivatized products were eluted at 38 °C, 0.7 mL/min by a 14 min linear gradient from 10 to 30% B and a subsequent 30% B wash for 18 min [buffer A, 140 mM sodium acetate, 27 μM EDTA, 0.17% (v/v) triethylamine adjusted to pH 5.0 with H_2PO_4; buffer B and 60% acetonitrile]. The amount of norleucine produced, monitored at 254 nm, was determined by comparison to a norleucine standard curve from 15 to 2000 pmol ($r^2 = 0.99$). Each reported value represents the average of 3−10 independent measurements and its standard deviation. The UV−vis spectra were measured as previously described (*14*). After recording the holoenzyme spectra, L-Met was added to a final concentration of 150 mM in 20 mM Hepes, pH 7.4, and 1 mm $CoCl_2$, and the spectra were rerecorded.

Computer Graphics. Atomic coordinates were superimposed with a six-dimensional search algorithm (*36*) or the SUPERIMPOSE program in the InsightII package (Biosym Technologies, San Diego/Molecular Simulations, Waltham, MA). Figures 2−5 and 8 were generated with BOBSCRIPT (*37*). Figure 6 was made by using MIDASPLUS (University of California, San Francisco Computer Graphics Laboratory).

RESULTS

Holoenzyme Active Site. The new expression system, purification scheme (*14*), and the optimization of crystal growth conditions made it possible to extend the resolution of the eMetAP crystal structure from 2.4 Å resolution (*4*) to 1.9 Å resolution. The best X-ray diffraction data sets were obtained from 1−3 week old crystals which grew readily from solutions containing freshly prepared Co(II), 15 mM methionine, and the detergent *N*-octanoyl sucrose. As indicated in Table 1, the new crystals have the same space group as previously reported (*4*), but have cell dimensions that differ by several angstroms.

The final model contains one molecule of MetAP (residues 2−263), 96 water molecules, three Co(II) ions, and one Na^+ ion in the asymmetric unit. The stereochemistry is good (Table 1). The catalytic center (Figure 2) is generated by strictly conserved residues among MetAPs that interact, in this case, with two Co(II) ions (Co1−Co2 distance = 3.2 Å) in a monodentate (His171 and Glu204) or a bidentate manner (Asp97, Asp108, and Glu235). Two solvent molecules (A and B) were clearly observed coordinated to the metal center (Figure 2A). The first of these bridges the cobalt ions. The second is a terminal ligand of Co2 and also participates in a hydrogen bond interaction with Thr99. The coordination geometry of Co1 is distorted trigonal bipyrimidal whereas that of Co2 is distorted octahedral (Figure 2B). $Asp108^{O\delta1}$ and $Glu204^{O\epsilon2}$ each occupy an axial position of Co1 while solvent A, $His171^{N\epsilon2}$, and $Glu235^{O\epsilon1}$ define the equatorial plane. The same shared solvent together with $Asp108^{O\delta2}$ and $Asp97^{O\delta1,O\delta2}$ make up the equatorial plane of Co2 while solvent B and $Glu235^{O\epsilon2}$ are in the axial positions. Several additional water molecules were observed in the active site (Figure 2B). Methionine, though present during crystallization, was not observed in the active site, suggesting that the enzyme has low affinity for the reaction product. An electron dense feature, presumably a third cobalt ion, was identified far from the active site at a crystal contact involving His54 and Glu123, a residue from the adjacent symmetry-related molecule. This was seen only in the holoenzyme structure (Table 1).

Cation-Binding Site. During the refinement of the holoenzyme structure, the thermal factor for a putative water molecule cradled within a turn containing residues 73−76 (Figure 3A) consistently refined to 1 $Å^2$, the lower limit in TNT, suggesting the presence of a more electron-dense atom. Test refinements with Na^+ and K^+ ions at this site showed that a sodium ion gave thermal factors that best matched those of the liganding oxygen atoms, suggesting that Na^+ is

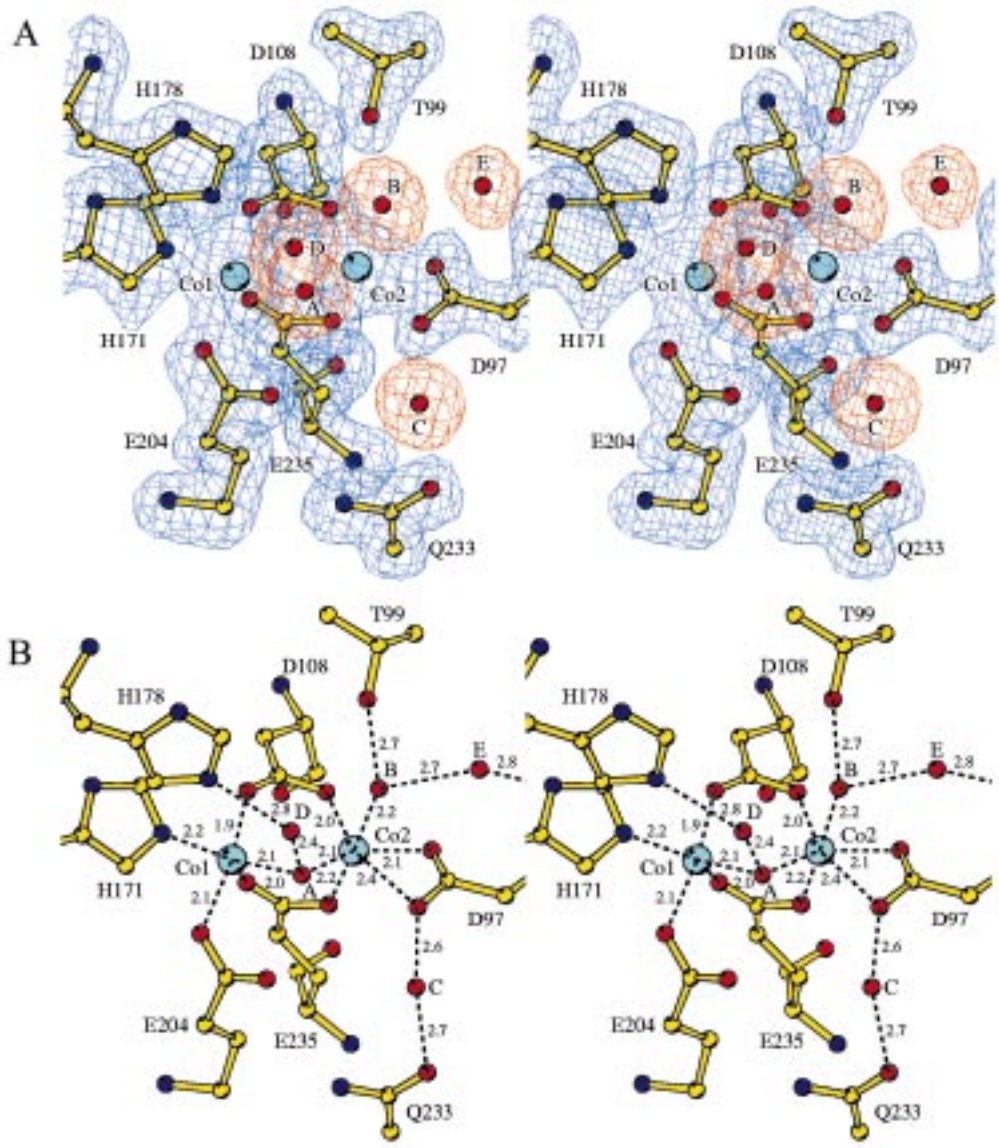

FIGURE 2: (A) Metal center of eMetAP. The stereo figure shows an "omit" $F_o - F_c$ electron density map calculated at 1.9 Å resolution in which the displayed residues were omitted from the refined model during map calculation. The map was contoured at 3σ where σ is the root-mean-square value of the electron density throughout the unit cell. To clarify the figure blue contours are used to show the protein atoms and the cobalt ions while red contours show the water molecules; both colors correspond to positive density. (B) Interatomic distances within the metal center. The distance between Co1 and Co2 is 3.2 Å. Color scheme for atoms: red, oxygen; blue, nitrogen; yellow, carbon; cyan, cobalt. Water molecules are labeled A to E.

present in all three structures. The three carbonyl-oxygen to metal ligand distances are consistent with Na^+ (*38*), but partial occupancy by K^+ cannot be ruled out. The location of this presumed sodium ion also corresponds with the thallium site used in the original structure determination (*4*). Indeed, thallium is routinely used as a Na^+ or K^+ mimic in crystallographic and biochemical experiments (*39*, *40*). The residue at the apex of the turn at the cation site, Asn74 in eMetAP, is strictly conserved among all enzymes exhibiting this protein fold, including MetAPs, creatinase, and ProAp (*5*, *7*). Asn74 has an unusual backbone conformation ($\phi = 42°$, $\psi = -108°$) that places this residue in a normally "disallowed" region of the Ramachandran plot.

Inhibitor Design and Mode of Binding. The natural aminopeptidase inhibitor, bestatin (*41*), has been used to design inhibitors of other aminopeptidases by changing the two specificity determinants: the side chain on the 2-hydroxy-3-amino acid metal chelator and the $P_1'-P_2'$ amino acids (*42*, *43*). To target eMetAP, a norleucine side chain was introduced as a mimic of the methionine side chain and alanine was placed in P_1', since eMetAP prefers small side chains in this position. The resulting amino acid, (3*R*)-amino-(2*S*)-hydroxyheptanoic acid (AHHpA) was used to synthesize the nonhydrolyzable transition-state analogue AHHpA-Ala-Leu-Val-Phe-OMe (Figure 1), which inhibited eMetAP with $IC_{50} = 5\ \mu M$ (*27*). Although the inhibitor's side chains and P_1' substituents are similar to those of a substrate for eMetAP, the stereochemistry is different (3R versus the natural configuration of S for methionine), and the peptide backbone is extended by one atom.

Crystals showing binding of the inhibitor could only be obtained by first preequilibrating the protein with inhibitor in solution (see Materials and Methods). In retrospect, this behavior is consistent with the substantial differences in cell dimensions between the free enzyme and the complex (Table 1). However, the 0.3 Å RMS difference between the C^α

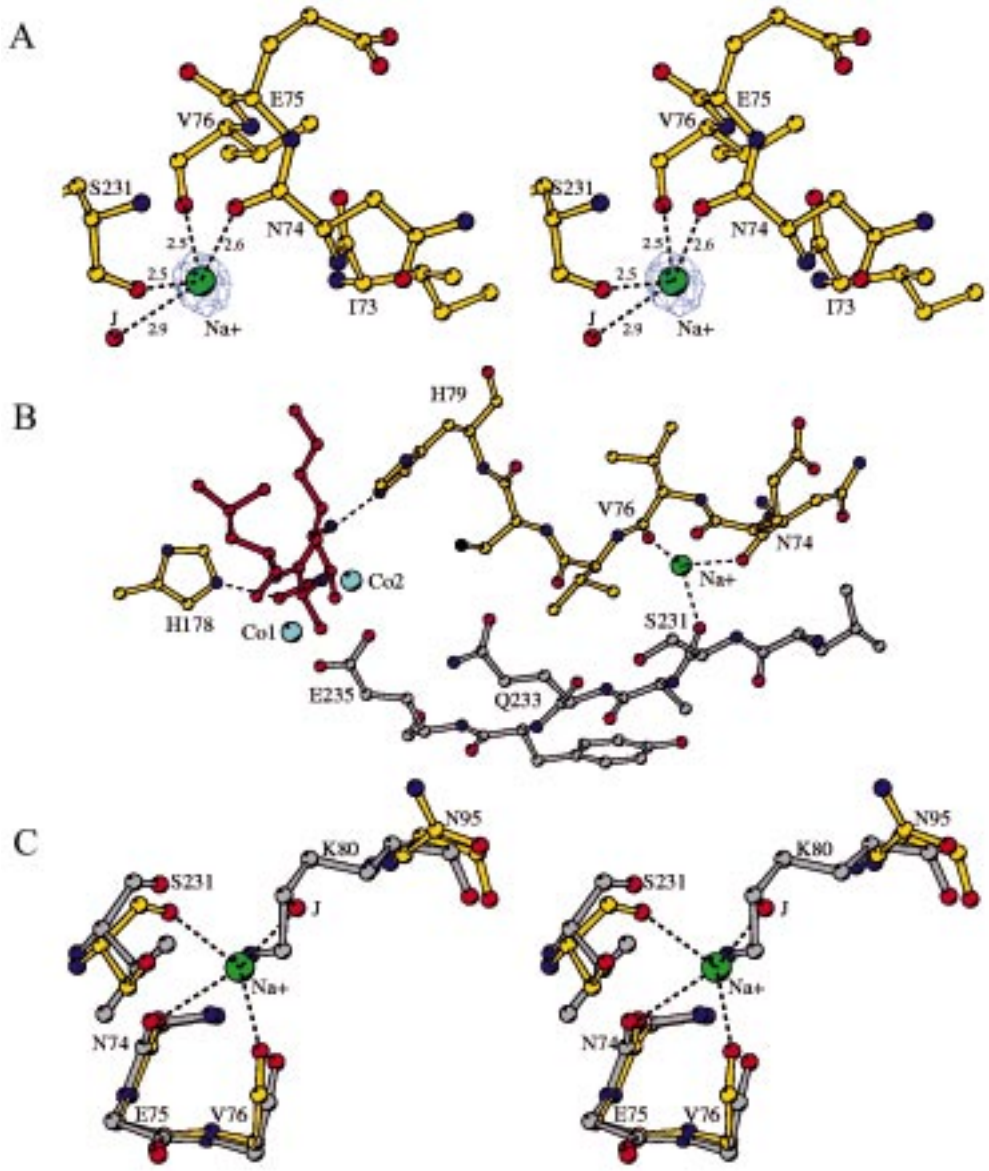

FIGURE 3: Monovalent cation binding site and its relationship to the metal center. (A) $F_o - F_c$ electron density map contoured at 10σ. The map (blue contours) was calculated to 2.0 Å resolution with the cation (green Na^+ atom) omitted from the refined model. (B) Proximity of the cation site to the metal center and the bound inhibitor (~13 Å). The cation site mediates an interaction between an N-terminal subdomain turn, near a solvent exposed loop containing His79, and a β-strand of the symmetry-related C-terminal subdomain (gray carbon atoms) that leads directly to one of the bridging carboxylate metal ligands (Glu235). (C) Superposition of the analogous turn from pfMetAP (gray carbon atoms, 1.2 Å RMS for the C^α atoms of the aminopeptidase domains and 0.6 Å for the C^α atoms of the loop and the residue equivalent to Ser231) (*5*). The positively charged N^ζ atom of Lys80 occupies a position analogous to the cation of eMetAP. The carbonyl oxygen atoms from Asn74, Val76, and Ser231 of eMetAP correspond to the carbonyl oxygen atoms from Asn57, Ile59, and Val277 of pfMetAP.

atoms of the holoenzyme and the inhibitor complex indicates no large conformational change associated with ligand binding. Clear density was present (Table 1, Figure 4) for the AHHpA-Ala-Leu moiety (Figure 1). The remaining atoms of the inhibitor are not observed presumably because they are poorly ordered.

The mode in which the inhibitor coordinates the dinuclear metal center is clearly seen and corresponds to the (2S,3R) enantiomer (Figure 4). The shortest ligand−metal distances are from the 2S-hydroxyl (O2) to each Co(II) ion as well as the 3R-amine to Co2. Comparison with the resting enzyme shows that solvents A, B, and D are displaced by the O2 hydroxyl, the N-terminal nitrogen, and the O1 atom of the inhibitor, respectively. Binding of the inhibitor also expands the coordination sphere of Co1 to distorted octahedral. In addition, Asp97 rotates slightly resulting in a longer $O^{\delta 2}$−Co2 interaction (2.7 versus 2.4 Å). A hydrogen-bonding network between the inhibitor backbone atoms and the protein is observed (Figure 4B). This network includes hydrogen bond interactions to His79 and His178, two absolutely conserved MetAP residues. The AHHpA side chain, analogous to methionine (Figure 1), fits snugly into a relatively hydrophobic P_1 pocket lined by residues His79, Cys59, Cys70, Tyr62, Tyr65, Phe177, and Trp221. The P_1' alanine side chain interacts with a shallow binding pocket primarily defined by Glu204, Gln233, Met206, and Tyr168.

Mutational Analysis of His79 and His178. Because of the conservation of His79 and His178, and their participation

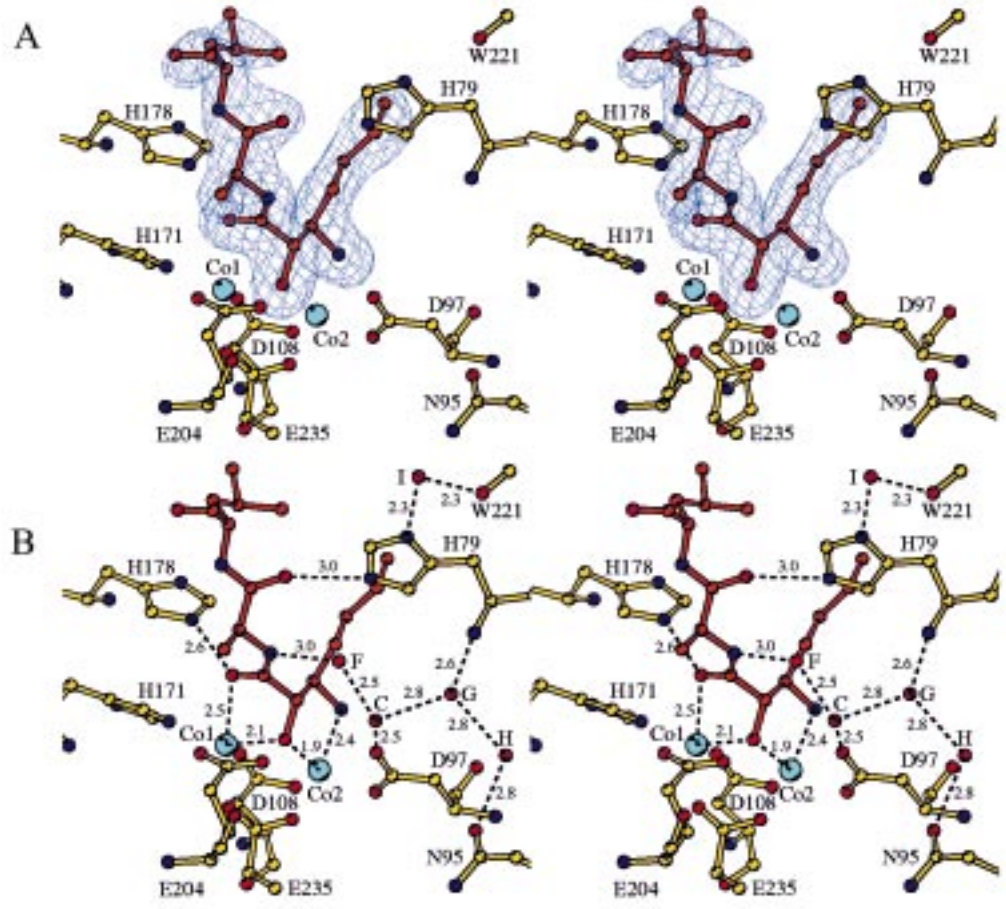

FIGURE 4: Interactions of the inhibitor in the active site. (A) $F_o - F_c$ electron density map contoured at 3σ. The map (blue contours) was calculated to 2.1 Å resolution with the inhibitor (orange bonds) omitted from the refined model during the map calculation. Gln233 and Thr99 are not displayed for clarity. (B) Selected interatomic distances. Dotted lines indicate interactions with the metal center as well as hydrogen bonding interactions between the inhibitor, adjacent water molecules and residues His79 and His178. Water molecules are labeled C and F to I.

in inhibitor binding (Figure 4B), these residues were individually mutated to alanine to investigate their potential roles in catalysis. The His178Ala mutant showed 50-fold lower activity toward Nle-Ala-Ala-Glu-Glu in comparison to the wild-type enzyme (97 ± 26 vs 5100 ± 580 nmol of Nle produced/min/mg in 0.2 mM $CoCl_2$). The His79Ala mutant was 5 orders of magnitude less active than wild-type enzyme [12 ± 2 pmol/min/mg with 100-fold more enzyme (150 μg), 1 mM $CoCl_2$, and 24 h incubation]. Similar results have been reported for the corresponding mutants in hMetAP (*19*).

The structure of the apo His79Ala mutant was determined crystallographically (Table 1). As shown in Figure 5A, the differences from the wild-type protein are modest, indicating that a major structural perturbation is not responsible for the almost complete loss in activity. Moreover, the locations of the metal ligands nearly superimposes with those of the wild-type holoenzyme, implying that the mutant enzyme is competent for metal binding. The electronic absorption spectra (Figure 5B) demonstrate that the His79Ala and His178Ala variants form nearly equivalent dinuclear metal centers as the wild-type enzyme. The addition of a high concentration of methionine to all three proteins also causes similar spectral perturbations which are consistent with conversion to octahedral Co(II) geometry for each metal center (*44*, *45*).

Choice of Metal at the Active Site. It has recently been reported that yMetAP-I reconstituted with low concentrations of Zn(II) is as active as the Co(II) enzyme (*15*). We found similar behavior with eMetAP, so long as the enzyme was treated with EDTA immediately prior to the activity measurement. Following this protocol, eMetAP showed nearly equivalent activity in the presence of 0.1 mM Co(II) (3420 ± 500 nmol/min/mg) or 0.1 mM Zn(II) (1010 ± 110 nmol/min/mg). However, in the presence of 1 mM zinc, the activity decreased by 7-fold (140 ± 23 nmol/min/mg). This observation is analogous to the finding that the yMetAP-I is inhibited by 1 mM zinc (*15*). Experiments are in progress to elucidate the structural basis for the observed decrease in activity at higher Zn(II) concentrations.

DISCUSSION

Methionine and proline aminopeptidases share the same general three-dimensional fold in their aminopeptidase domains (*4*−*6*, *11*). In particular, the ligands to the dinuclear metal center and two histidine residues, His79 and His178 in eMetAP, are conserved (*5*, *7*). Catalytic activity has been observed for enzymes in which the metal center was comprised of Co(II) or Zn(II) for eMetAP; Co(II), Zn(II), Mn(II), or Ni(II) for yMetAP-I; Co(II) for yMetAP-II; Co(II) for hMetAP-II and Mn(II) for ProAP (*11*, *15*, *16*, *19*). Therefore, the following discussion, while based on cobalt-

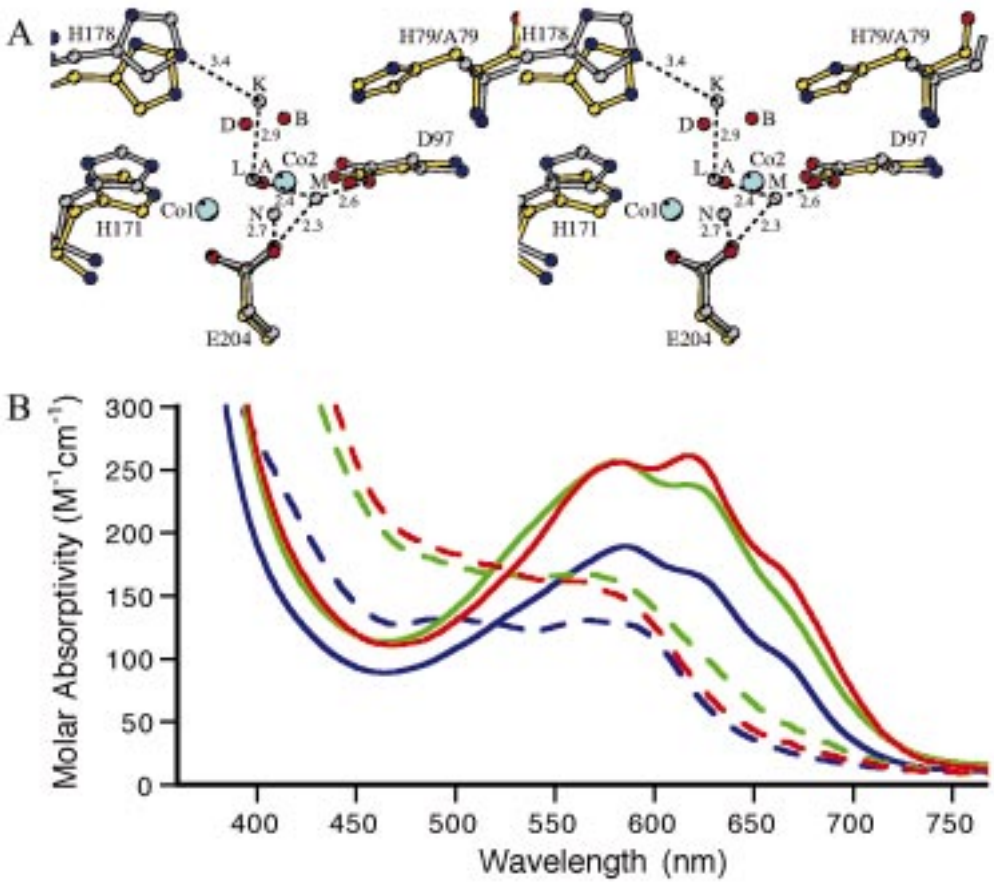

FIGURE 5: (A) Comparison of eMetAP holoenzyme to the apoenzyme-form of the His79Ala mutant (RMS of the C^{α} atoms 0.9 Å, residues 2−262). Solvent L corresponds to solvent A, the metal-bridging ligand of the holoenzyme. Solvent M interacts via hydrogen bonds with Asp97 and Glu204. (B) Electronic absorption spectra for the Co(II)-substituted eMetAPs; wild-type (blue), His79Ala (red), and His178Ala (green) variants of eMetAP. Protein concentrations were in the range 0.6−2.6 mM and absorptivities were normalized to be on a molar basis. Solid and dashed lines indicate the absence or presence of 150 mM L-Met, respectively, in 20 mM Hepes, pH 7.4, and 1 mM $CoCl_2$. Over the range of wavelengths included, the spectrum of a solution of 150 mM methionine in 20 mM Hepes and 1 mM $CoCl_2$, pH 7.4, is indistinguishable from the baseline (not shown).

substituted eMetAP, should be relevant to all enzymes displaying this protein fold.

The inhibitor complex of eMetAP provides a structural basis for the known substrate preferences of MetAPs. The interaction of the terminal nitrogen of the inhibitor with Co2 (Figure 4B) is consistent with the requirement for a free amino-terminus. The tapered shape of the hydrophobic pocket is consistent with the requirement for methionine at the P_1 position and explains the inability of the enzyme to cleave substrates containing methionine sulfoxide (*1*). The limited amount of space at the P_1' site (defined by the side chains of Glu233, Met206, and Tyr168) is in agreement with the preference for substrates with small side chains at this position (*1*, *46*, *47*).

The apparent effectiveness and specificity of the AHHpA-containing inhibitor toward eMetAP suggests that it may represent another important class of therapeutic compounds for combating angiogenesis in cancer and other noncancerous diseases of aberrant vascularization (*21*, *48*). Reports showing the lethality of deleting the MetAP gene from *E. coli* and both MetAP (I and II) genes from yeast also indicate that these compounds could be beneficial as antimicrobial and antifungal agents (*49*, *50*).

Mechanism of Catalysis. The higher resolution of eMetAP diffraction data permitted observation of the solvent structure within the active site (Figure 2). In common with *Pyrococcus furiosis* MetAP (pfMetAP) and ProAP, a solvent molecule or μ-hydroxide ion is bound between the ions of the dinuclear metal center (*5*, *11*). Such bridging ligands typically mediate metal−metal interactions (*8*). It seems highly likely that this bridging moiety is a key structural feature with respect to catalysis for MetAPs. The binding of the inhibitor to the metal center displaces both the bridging and terminal solvent moieties and increases the coordination number of Co1 (Figure 4). This binding mode suggests a structural rationale for how a substrate and subsequent reaction intermediate(s) may interact with the metal center. The change in the electronic absorption spectra of the wild-type and mutant proteins upon the addition of methionine also supports product interactions with both Co(II) ions (Figure 5). The available data suggest two possible transition states (Figure 6) corresponding to two slightly different reaction mechanisms (Figure 7). These are briefly outlined below, followed by a discussion of the evidence for the respective schemes and comparisons to LeuAP and creatinase.

Mechanism I. One possible transition state is shown in Figure 6A with the corresponding reaction scheme shown in Figure 7. This model was constructed with the following assumptions: (i) that the N-terminus of the substrate coordinates to Co2 at the expense of the terminal solvent

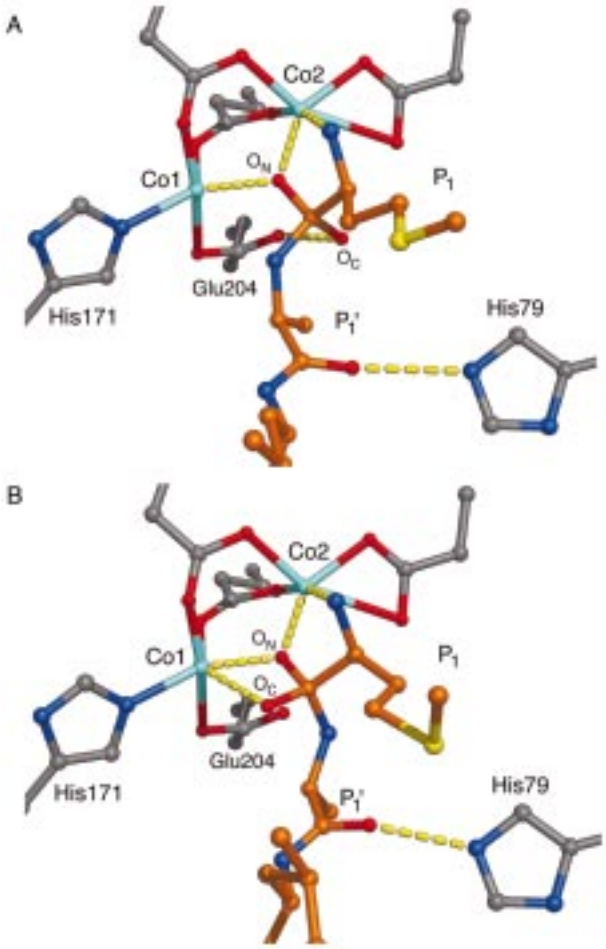

FIGURE 6: Models for the reaction intermediates of eMetAP. The oxygen atoms are labeled according to their proposed origin: O_N, attacking nucleophile; O_C, the substrate carbonyl oxygen. His79 interacts with the inhibitor (3.0 Å, Figure 3) and the transition state models in a similar fashion (2.6−2.8 Å). Coordinating ligands to the metals are shown by solid bonds. Potential metal, hydrogen bonding, and transitional interactions are indicated by dashed yellow lines. The hypothetical transition state models were built and energy minimized by the BUILDER and DISCOVER programs within the InsightII package (Biosym Technologies, San Diego/Molecular Simulations, Waltham, MA) assuming the formation of a tetrahedral *gem*-diolate intermediate. Only small rotations about the $C^{\alpha}-C^{\beta}$ and the C^{α}-amide nitrogen bonds of P_1' were needed to dock the model into the active site of the eMetAP−inhibitor complex. (A) Model 1. In this model, His178, which has been omitted for clarity, could potentially form interactions with the backbone nitrogens of the P_1' (3.5 Å) and P_2' (3.1 Å) residues. (B) Model 2. In this case, His178 may also help to stabilize the carboxyanion of the intermediate (3.3 Å) or interact with the P_2' (3.5 Å) backbone nitrogen.

molecule B, (ii) the formation of a noncovalent tetrahedral *gem*-diolate intermediate, (iii) that the original carbonyl oxygen (O_C) of the scissile peptide bond interacts with Glu204, and (iv) that the water or μ-hydroxo moiety (solvent A) of the resting enzyme (Figure 2) represents the nucleophile (O_N). In this mechanism, the solvent−amine ligand exchange could alter the electronic character of the dinuclear metal center (Figure 7, path A) and facilitate proton transfer from the μ-hydroxide to the carbonyl group (O_C) resulting in a hydrogen-bonding interaction with Glu204. At the same time, oxygen O_N would attack the carbonyl carbon of the scissile bond leading to the tetrahedral intermediate. Collapse of the intermediate could be facilitated by His178 acting as a proton donor (3.5 Å away) to the leaving group amino nitrogen. The role of His79 in this scheme is to orient the substrate in a productive manner for catalysis.

Mechanism II. The second possible transition state, shown in Figure 6B, was built using the same assumptions as the first. The essential difference is that the plane of the former peptide bond has been rotated to enable the O_C atom of the intermediate to interact with Co1. In this orientation, O_C is 2.7 Å from Co1 and is also fairly close (3.3 Å) to His178. In the corresponding mechanism (Figure 7, path B), ligand exchange at the metal center functions to activate the μ-hydroxide for nucleophilic attack. The resultant tetrahedral intermediate is stabilized by chelation to Co1 and possible hydrogen bonding with His178. Analogous mechanistic features have been suggested for ProAP (*11*). The location of Glu204 and its proximity to the nitrogen of the scissile bond (2.7 Å), suggest that this residue might shuttle a proton from the attacking μ-hydroxide to the leaving nitrogen. In this scenario, Glu204 of eMetAP plays a role analogous to that proposed for Glu143 of thermolysin (*51*−*53*), Glu270 of carboxypeptidase (*52*, *54*), Asp128 of arginase (*13*) and possibly Glu151 of the aminopeptidase from *Aeromonas proteolytica* (*55*, *56*). All of these are metalloproteases with three-dimensional structures apparently unrelated to that of eMetAP. Although the idea of related mechanisms of action for these different metalloenzymes is very attractive, one cannot rule out the possibility, in the case of eMetAP, that His79 or His178 might also act as proton donors, either directly or via solvent. For example, these histidines may transfer a proton, in an analogous manner proposed for His141 in arginase, to the newly released N-terminus (*13*).

Comparison of the Reaction Schemes. One of the main differences between the two mechanisms proposed for MetAP is the location of the O_c atom of the substrate upon binding (Figures 6 and 7). Associated with this, the prochiral carbonyl group is attacked, respectively, on its si or re enantiotopic face in mechanism I and II. The role of His178 is also different. In mechanism I, His178 is proposed to protonate the leaving group, whereas in mechanism II, it may ameliorate the stabilization of the carboxyanion of the transition state by Co1. The significant residual activity of the His178Ala mutant, however, suggests that His178 is not critical for catalysis. This observation tends to argue against mechanism I. Additional support for mechanism II comes from the mode of binding adopted by the inhibitor. In the complex (Figure 4B), two oxygens atoms chelate Co1, completing the coordination sphere from a distorted trigonal bipyramid to distorted octahedral. This is analogous to the proposed transition state in mechanism II (Figures 6B and 7).

The importance of His79 in the mechanism of action of eMetAP is highlighted by the almost complete loss of activity of the His79Ala mutant. Since His79 is, however, assumed to play an equivalent role in the two alternative mechanistic schemes, the low activity of the mutant does not help to differentiate between them. The inability of the mutant to form a hydrogen bond to the P_1' carbonyl oxygen atom of the substrate may prevent binding of the substrate in a productive manner. This suggests that, even though substrates likely bind to the metal center via their N-termini, interactions remote from the scissile bond play a major role in catalysis.

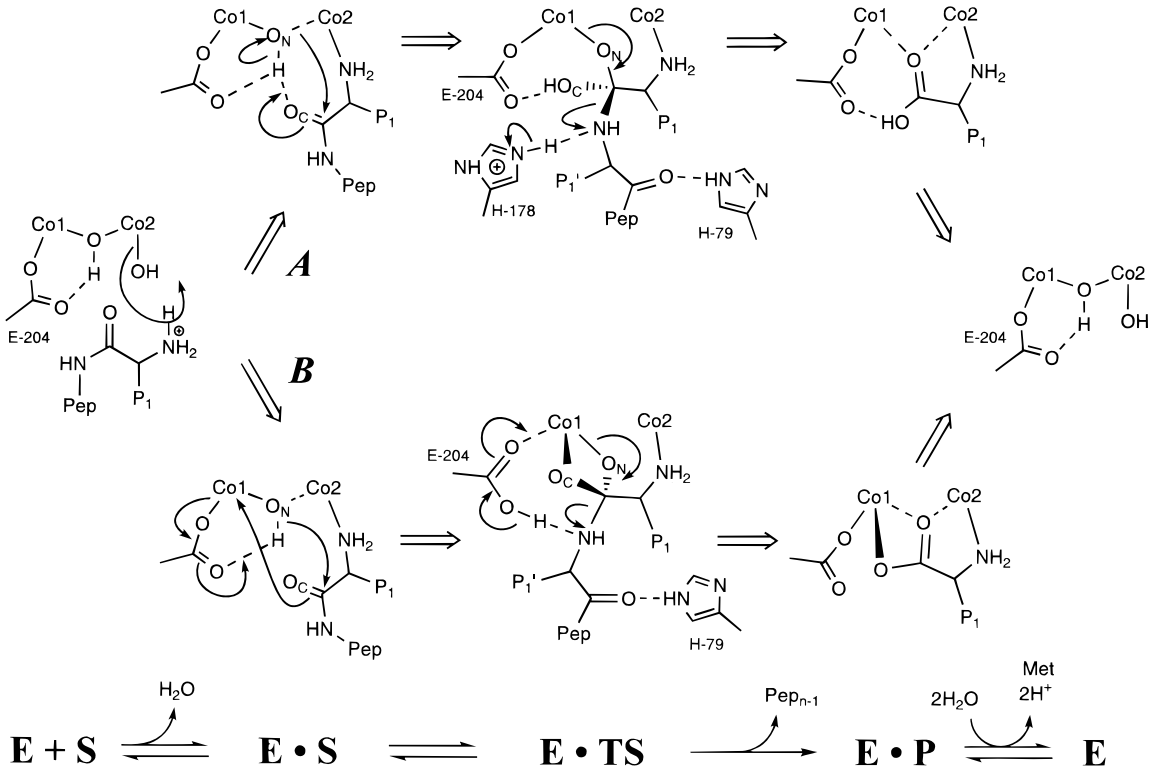

FIGURE 7: Two proposed reaction mechanisms for eMetAP catalysis. In mechanism I (path A) the tetrahedral intermediate is stabilized by interactions with Glu204 and the metal center. In mechanism II (path B), the tetrahedral intermediate is stabilized by the chelation of Co1 and potential hydrogen bonding with His178. His79 interacts with the backbone P_1' carbonyl atom of the substrate in both schemes (see Discussion).

It is tempting to speculate that the monovalent cation site (Figure 3A) may also play a part in the function of His79. The sodium binding site is formed by the juxtaposition of backbone carbonyl groups from residue 231 in a β-strand and residues 74 and 76 in a tight turn. Amino acids within the turn are highly conserved within the MetAP family (*5*, *7*). The proximity of the Na^+ site (Figure 3B) to His79 and the two cobalt ions (~13 Å) suggests that it may mediate an interaction between the subdomains of the folded protein, thus stabilizing the metal center and/or positioning the solvent accessible loop containing His79 for catalysis. Interestingly, a comparison of this unusual turn with that seen in pfMetAP (*5*) shows the cation to be replaced by the positively charged N^{ζ} atom of Lys80 in pfMetAP (Figure 3C). Sequence alignments suggest that a similar lysine-based interaction occurs in hMetAP-II and yMetAP-II (*5*−*7*). It might also be noted that similarly arranged backbone carbonyl atoms are used to bind monovalent cations in a number of other proteins (*57*) including dialkylglycine decarboxylase (*58*), subtilisin (*59*), cytochrome *c* peroxidase (*60*), and cytochrome P450cam (*61*).

Comparison with Leucine Aminopeptidase. The overall fold of bovine LeuAP is unrelated to that of eMetAP (*9*, *10*, *22*), but the enzyme does have a dinuclear metal center containing a bridging μ-hydroxide ion. Notwithstanding the different protein fold, metal ligands, and coordination geometry, the backbone atoms of the natural product amastatin bound to LeuAP (*23*) superimpose within 0.5 Å of the analogous atoms of AHHpA analogue bound to eMetAP (Figure 8A). The metal interactions of the respective inhibitors are quite similar; the N-terminus interacts with Co2/Zn2, the O2 hydroxyl group bridges the two metal ions, and the O1 carbonyl atom interacts with Co1/Zn1. In addition, $Lys262^{N\epsilon}$ and the backbone nitrogen of $Gly262^{N}$ make interactions similar to His178 and His79, respectively. Significant differences are also apparent; for example, there is no counterpart to Glu204 (not shown), and Lys262 is thought to act as a proton shuttle (*9*, *10*). Thus, although eMetAP and LeuAP are both metalloaminopeptidases, they do appear to have evolved somewhat different mechanisms of action.

The comparison between the binding modes of the inhibitors to eMetAP and LeuAP helps explain why amastatin and bestatin are poor inhibitors of MetAP. These natural products both contain C^{γ}-branched amino acid side chains (Phe or Leu) at the N-terminus. An apparent steric clash between these branched side chains and Phe177 and Cys59 of eMetAP would tend to prevent binding to eMetAP. In a similar manner, the shallow pocket primarily generated by residues Gln233, Met206, and Tyr168 would tend to prevent the binding of the P_1' leucine residue of bestatin.

Relationship between MetAP and Creatinase. It was previously shown that creatinase and eMetAP share the same overall "pita-bread" fold (*7*, *24*). Creatinase hydrolyzes the guanidinium group of creatine, which is reminiscent of a peptide bond. In contrast, however, the enzyme lacks the metal ions that are essential to the activity of all of the MetAPs. The availability of the structure of the inhibitor complex of eMetAP now makes it possible to compare the active-site regions of the respective enzymes in detail.

Figure 8B shows the carbamyl sarcosine complex of creatinase superimposed on the inhibitor complex of eMetAP. Although the superposition is based on the backbone atoms of the respective proteins, the carbon atoms attacked by the nucleophile during the reaction (or at least their counterparts in the inhibitors) are within 1.0 Å of each other. In addition,

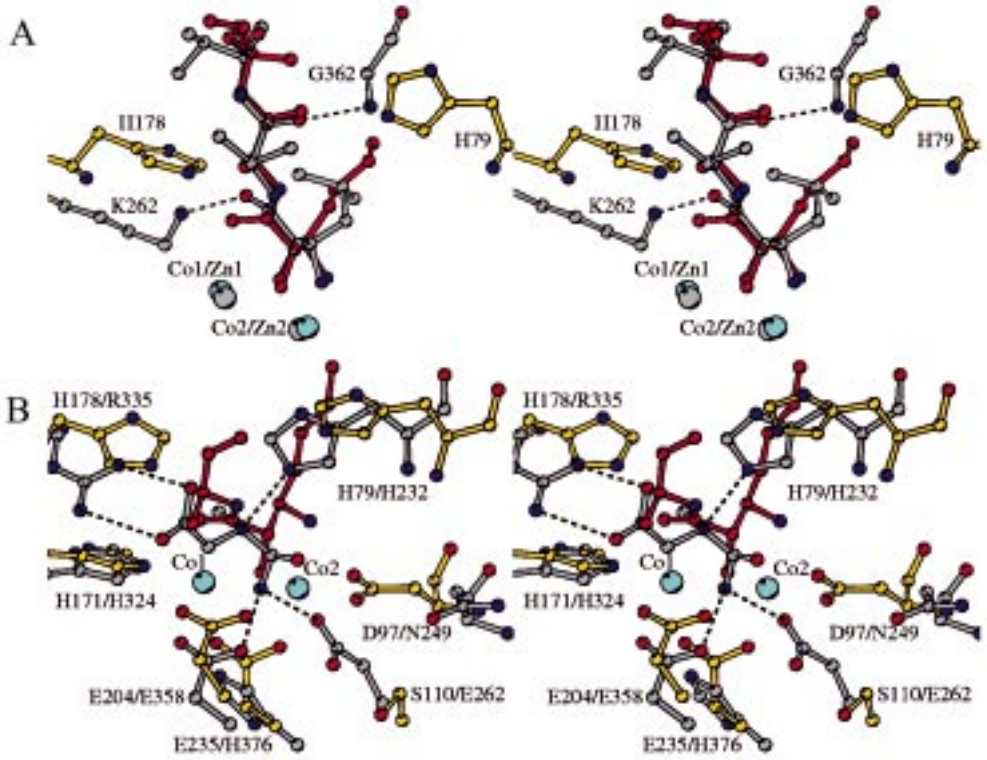

FIGURE 8: (A) Comparison of the eMetAP−inhibitor complex (yellow and orange bonds) with amastatin bound to LeuAP (gray bonds) [(*23*) PDB accession code 1BLL]. The mainchain atoms of the inhibitor plus the metal ions, a total of 28 atoms, superimpose with a RMS discrepancy of 0.5 Å. Dashed lines indicate LeuAP protein−inhibitor interactions. (B) Comparison of the eMetAP inhibitor complex (orange and yellow bonds) with the carbamyl−sarcosine complex of creatinase (gray) [(*24*) PDB accession code 1CHM]. The superposition is based on the C^{α} atoms within the C-terminal domain of creatinase, which have a RMS discrepancy of 1.5 Å with the corresponding atoms in eMetAP (*7*). The atom labels indicate the eMetAP/creatinase residues. Interactions between carbamyl sarcosine and creatinase are shown as dashed lines. His232, equivalent to His79 in eMetAP, makes a hydrogen-bonding interaction to the backbone nitrogen of carbamyl sarcosine.

the structure of the carbamyl group is remarkably similar to the transition state proposed for mechanism I of eMetAP. Several important differences, however, occur between the two structures. For example, the interaction between the hydroxyl oxygen (O2) of the MetAP inhibitor and the two positively charged cobalt ions is replaced by an interaction between the carbamyl nitrogen, which may be positively charged, and two acidic groups (Glu262 and Glu358) of creatinase. His178 of eMetAP, which is conserved in all methionine aminopeptidases, is replaced in creatinase by Arg335, which forms a key salt bridge with the carboxylate of the inhibitor. His79 of eMetAP, conserved in all MetAPs, is analogous to His232 in creatinase. Moreover, His232 makes a hydrogen bond to the nitrogen of the surrogate scissile bond (Figure 8B) in carbamyl sarcosine.

Possible mechanistic parallels between MetAPs and creatinase are outlined below. First, since the respective enzymes are likely to have diverged from a common precursor, they may have retained common catalytic features. The apparent close superposition of the atoms mimicking the carbon atom attacked during catalysis supports this contention. Glu358 of creatinase (analogous to Glu204 of eMetAP) is proposed to help bind the guanidinium group of the substrate. Although Glu358 is apparently close to the nitrogen of the scissile bond, its possible role as a proton shuttle, similar to Glu204 in mechanism II of eMetAP, has not been suggested (*24*). It is also noteworthy that His178, which is not absolutely essential for the activity of eMetAP, is replaced by an arginine (Arg335) in creatinase. His79, which clearly is important in the activity of eMetAP, is retained in creatinase (His232), suggesting that this residue may play an equivalent and/or essential role in the activity of both enzymes. His232 in creatinase is thought to be critical for activating a water molecule for nucleophilic attack, binding of the substrate, and shuttling a proton (*24*). At this point, it is unclear whether steric restrictions imposed by the larger MetAP substrate (in particular the presence of the amino acid at the P_1' position) would prevent His79 from interacting with the nitrogen of the scissile bond in a manner analogous to that observed in creatinase. If such an interaction were to occur, the proposed function of His79 in eMetAP, to facilitate the proper binding of substrates, may need to be expanded to include a role as a potential proton donor to the amino leaving group.

ACKNOWLEDGMENT

We gratefully acknowledge Drs. L. Weaver, D. Tronrud, M. Quillin, M. Sagermann, I. Korndörfer, and D. Juers for their assistance in all aspects of data collection, model building and refinement.

REFERENCES

1. Ben-Bassat, A., Bauer, K., Chang, S. Y., Myambo, K., Boosman, A., and Chang, S. (1987) *J. Bacteriol. 169*, 751−757.
2. Bradshaw, R. A., Brickey, W. W., and Walker, K. W. (1998) *Trends Biochem. Sci. 23*, 263−267.
3. Arfin, S. M., Kendall, R. L., Hall, L., Weaver, L. H., Stewart, A. E., Matthews, B. W., and Bradshaw, R. A. (1995) *Proc. Natl. Acad. Sci. U.S.A. 92*, 7714−7718.

4. Roderick, S. L., and Matthews, B. W. (1993) *Biochemistry 32*, 3907−3912.
5. Tahirov, T. H., Oki, H., Tsukihara, T., Ogasahara, K., Yutani, K., Ogata, K., Izu, Y., Tsunasawa, S., and Kato, I. (1998) *J. Mol. Biol. 284*, 101−124.
6. Liu, S., Widom, J., Kemp, C. W., Crews, C. M., and Clardy, J. (1998) *Science 282*, 1324−1327.
7. Bazan, J. F., Weaver, L. H., Roderick, S. L., Huber, R., and Matthews, B. W. (1994) *Proc. Natl. Acad. Sci. U.S.A. 91*, 2473−2477.
8. Holm, R. H., Kennepohl, P., and Solomon, E. I. (1996) *Chem. Rev. 96*, 2239−2314.
9. Strater, N., and Lipscomb, W. N. (1995) *Biochemistry 34*, 14792−14800.
10. Strater, N., and Lipscomb, W. N. (1995) *Biochemistry 34*, 9200−9210.
11. Wilce, M. C., Bond, C. S., Dixon, N. E., Freeman, H. C., Guss, J. M., Lilley, P. E., and Wilce, J. A. (1998) *Proc. Natl. Acad. Sci. U.S.A. 95*, 3472−3477.
12. Scolnick, L. R., Kanyo, Z. F., Cavalli, R. C., Ash, D. E., and Christianson, D. W. (1997) *Biochemistry 36*, 10558−10565.
13. Kanyo, Z. F., Scolnick, L. R., Ash, D. E., and Christianson, D. W. (1996) *Nature 383*, 554−557.
14. Lowther, W. T., McMillen, D. A., Orville, A. M., and Matthews, B. W. (1998) *Proc. Natl. Acad. Sci. U.S.A. 95*, 12153−12157.
15. Walker, K. W., and Bradshaw, R. A. (1998) *Protein Sci. 7*, 2684−2687.
16. Griffith, E. C., Su, Z., Turk, B. E., Chen, S., Chang, Y. H., Wu, Z., Biemann, K., and Liu, J. O. (1997) *Chem. Biol. 4*, 461−471.
17. Sin, N., Meng, L., Wang, M. Q., Wen, J. J., Bornmann, W. G., and Crews, C. M. (1997) *Proc. Natl. Acad. Sci. U.S.A. 94*, 6099−6103.
18. Zetter, B. R. (1998) *Annu. Rev. Med. 49*, 407−424.
19. Griffith, E. C., Zhuang, S., Niwayama, S., Ramsay, C. A., Chang, Y., and Liu, J. O. (1998) *Proc. Natl. Acad. Sci. U.S.A. 95*, 15183−15188.
20. Ingber, D., Fujita, T., Kishimoto, S., Sudo, K., Kanamaru, T., Brem, H., and Folkman, J. (1990) *Nature 348*, 555−557.
21. Folkman, J. (1995) *Nat. Med. 1*, 27−31.
22. Burley, S. K., David, P. R., Sweet, R. M., Taylor, A., and Lipscomb, W. N. (1992) *J. Mol. Biol. 224*, 113−140.
23. Kim, H., and Lipscomb, W. N. (1993) *Biochemistry 32*, 8465−8478.
24. Coll, M., Knof, S. H., Ohga, Y., Messerschmidt, A., Huber, R., Moellering, H., Russmann, L., and Schumacher, G. (1990) *J. Mol. Biol. 214*, 597−610.
25. Schechter, I., and Berger, A. (1967) *Biochem. Biophys. Res. Comm. 27*, 157−162.
26. Lim, S., and Rich, D. H. (1994) in *Petides: Chemistry, Structure and Biology* (Hodges, R. S., and Smith, J. A., Eds.) pp 625−627, ESCOM, Leiden, The Netherlands.
27. Keding, S. J., Dales, N. A., Lim, S., Beaulieu, D., and Rich, D. H. (1998) *Synth. Commun. 28*, 4463−4470.
28. Otwinowski, Z., and Minor, W. (1997) *Methods Enzymol. 276*, 307−326.
29. Navaza, J. (1994) *Acta Crystallogr., Sect. A 50*, 157−163.
30. Sack, J. S., and Quiocho, F. A. (1997) *Methods Enzymol. 277*, 158−172.
31. Jones, T. A., Zou, J. Y., Cowan, S. W., and Kjeldgaard. (1991) *Acta Crystallogr., Sect. A 47*, 110−119.
32. Tronrud, D. E. (1997) *Methods Enzymol. 277*, 306−319.
33. Ricci, J., Bousvaris, A., Taylor, A., and Umezawa, H. (1981) *Acta Crystallogr., Sect. A 37*, C61.
34. Tronrud, D. E. (1996) *J. Appl. Crystallogr. 29*, 100−104.
35. Zuo, S., Guo, Q., and Chang, Y. (1994) *Anal. Biochem. 222*, 514−516.
36. Diederichs, K. (1995) *Proteins 23*, 187−195.
37. Esnouf, J. (1997) *J. Mol. Graph. 15*, 132−138.
38. Carrell, C. J., Carrell, H. L., Erlebacher, J., and Glusker, J. P. (1988) *J. Am. Chem. Soc. 110*, 8651−8656.
39. Badger, J., Li, Y., and Caspar, D. L. D. (1994) *Proc. Natl. Acad. Sci. U.S.A. 91*, 1224−1228.
40. Pedersen, P. A., Nielsen, J. M., Rasmussen, J. H., and Jorgensen, P. L. (1998) *Biochemistry 37*, 17818−17827.
41. Suda, H., Takita, T., Aoyagi, T., and Umezawa, H. (1976) *J. Antibiot. 29*, 100−102.
42. Rich, D. H., Moon, B. J., and Harbeson, S. J. (1984) *J. Med. Chem. 27*, 417−422.
43. Ocain, T. D., and Rich, D. H. (1988) *J. Med. Chem. 31*, 2193-2199.
44. Bertini, I., and Luchinat, C. (1984) *Adv. Inorg. Biochem. 6*, 71−111.
45. Maret, W., and Vallee, B. L. (1993) *Methods Enzymol. 226*, 52−71.
46. Sherman, F., Stewart, J. W., and Tsunasawa, S. (1985) *BioEssays 3*, 27−31.
47. Walker, K. W., and Bradshaw, R. A. (1999) *J. Biol. Chem. 274*, 13403−13409.
48. Folkman, J. (1995) *N. Engl. J. Med. 333*, 1757−1763.
49. Chang, S. Y., McGary, E. C., and Chang, S. (1989) *J. Bacteriol. 171*, 4071−4072.
50. Li, X., and Chang, Y. H. (1995) *Proc. Natl. Acad. Sci. U.S.A. 92*, 12357−12361.
51. Hangauer, D. G., Monzingo, A. F., and Matthews, B. W. (1984) *Biochemistry 23*, 5730−5741.
52. Monzingo, A. F., and Matthews. B. W. (1984) *Biochemistry 23*, 5724−5729.
53. Matthews, B. W. (1988) *Acc. Chem. Res. 21*, 333−340.
54. Christianson, D. W., and Lipscomb, W. (1989) *Acc. Chem. Res. 22*, 62−69.
55. Chevrier, B., D'Orchymont, H., Schalk, C., Tarnus, C., and Moras, D. (1996) *Eur. J. Biochem. 237*, 393−398.
56. Chen, G., Edwards, T., D'souza, V. M., and Holz, R. C. (1997) *Biochemistry 36*, 4278−4286.
57. Chakrabarti, P. (1990) *Biochemistry 29*, 651−658.
58. Toney, M. D., Hohenester, E., Cowan, S. W., and Jansonius, J. N. (1993) *Science 261*, 756−759.
59. McPhalen, C. A., and James, M. N. (1988) *Biochemistry 27*, 6582−6598.
60. Miller, M. A., Han, G. W., and Kraut, J. (1994) *Proc. Natl. Acad. Sci. U.S.A. 91*, 11118−11122.
61. Vidakovic, M., Sligar, S. G., Li, H., and Poulos, T. L. (1998) *Biochemistry 37*, 9211−9219.

BI990684R